36a.0 RATIONALIZATION OF LIQUID/SOLID AND SOLID/SOLID INTERPHASE INSTABILITIES DURING THERMAL-MECHANICAL TRANSIENTS OF METAL ADDITIVE MANUFACTURING

Alec Saville (Mines)
Faculty: Amy Clarke (Mines)
Other Participants: Jonah Klemm-Toole, Jeremy Shin, and Brian Rodgers (Mines)
Industrial Mentor: TBD

This project initiated in Fall 2018 and is supported by the Office of Naval Research. The research performed during this project will serve as part of the basis for a Ph.D. thesis program for Alec Saville, with future work being transitioned to Jeremy Shin and Brian Rodgers in coming reporting periods.

36a.1 Project Overview and Industrial Relevance

Over the last decade, metallic additive manufacturing (AM) has seen increasing use in the creation of near-net shape functional and low-risk structural components. The primary benefit of AM over traditional processing is the ability to create custom geometries beyond what is possible with traditional manufacturing and reduce the waste associated with extensive machining [36.1-4]. One of the primary challenges to this production technique is maintaining control of material properties and microstructure via careful selection/maintenance of build parameters. Porosity, cracking, anisotropic loading response, and detrimental microstructural formations are all possible defects in AM builds, leading to a limited scope of application for metallic AM [36.5-8]. The influence of processing parameters (e.g., scan strategy or layer thickness) on material performance, microstructural evolution, and defect formation is not well-understood and is an active area of materials research.

This project focuses on analyzing AM Ti-6Al-4V produced via an electron beam melted (EBM) powder process to evaluate the influence of processing conditions on crystallographic texture and anisotropic loading responses. Three specimens of EBM Ti-6Al-4V were produced at Oak Ridge National Laboratory (ORNL) with different scan strategies, identified by the names Raster, Dehoff, and Random. Random and Dehoff are spot deposition methods, depositing material in spots instead of in a linear fashion (**Figure 36.1)**. Raster is a deposition strategy commonly used in industry where material is deposited linearly every layer and the travel path rotated 67.5° between layers (**Figure 36.2)**.

These scan strategies altered the local thermal history of each build and gave rise to potentially different crystallographic texture. Differences in texture are important to controlling anisotropic behavior in AM builds, and by quantifying these differences this work aims to develop a greater understanding of how anisotropic behavior evolves for AM metallic systems.

36a.2 Previous Work

36a.2.1 Literature Review of AM of Ti-6Al-4V

A survey of AM literature pertaining to Ti-6Al-4V and EBM build processes was completed to give a general background for future work. EBM Ti-6Al-4V differs microstructurally from selective laser melting (SLM) processes due to decreased cooling rates as a result of the heated build chambers intrinsic to electron beam AM machines. EBM builds exhibit colony $\alpha + \beta$ microstructures with potential Widmansttatten α or martensitic α' depending on build chamber temperature and build parameters [36.4, 36.9-11], while laser builds exhibit an almost completely martensitic microstructure. This latter microstructure forms due to the lack of a heated chamber in SLM builds, resulting in an increased cooling rate and thus a microstructure dominated by α' [36.12-16].

It is worth noting EBM builds are thought to exhibit an α' microstructure directly after the initial deposition of a layer of material. This is decomposed into a fine $\alpha + \beta$ lamellae during subsequent layer depositions due to higher ambient temperature, and has been shown to increase both ductility and strength of Ti-6Al-4V [36.5]. SLM builds can achieve similar microstructures through careful manipulation of build parameters, but is a more involved process than that seen naturally in EBM. [36.17-18]

Crystallographic texture for AM Ti-6Al-4V is normally fairly weak. Directly after deposition, a strong cubic solidification {001} fiber texture is exhibited by the β-Ti phase. After cooling below the β-transus temperature, most β-Ti transforms into α-Ti with relatively weak texture. With the next deposition pass, the newly deposited material solidifies as β-Ti and grows epitaxially on previously deposited layers heated into the β-regime. This process effectively cycles the previous few layers of a Ti-6Al-4V build through a repeated $\beta \leftrightarrow \alpha$ transformation, removing significant α-Ti texture [36.5, 36.19-20]. Thus, relatively weak α-Ti texture is expected.

36a.2.2 Neutron Diffraction Experiments and Training on Processing Neutron Diffraction Data

Neutron diffraction data was collected in Q3-2018 at the Los Alamos Neutron Science Center's High Pressure-Preferred Orientation (LANSCE-HIPPO) beamline for the Random, Raster, and Dehoff specimens. Both bulk and local diffraction experiments were completed (Figure 36.2) to collect crystallographic texture information that can be compared between specimens and as a function of build height. In Q4-2018 to Q2-2019, training on processing neutron diffraction data using the Material Analysis Using Diffraction (MAUD) software package was also completed via the guidance of Los Alamos National Laboratory (LANL) scientists, laying the groundwork for the recent progress reported below.

36a.3 Recent Progress

36a.3.1 Processing of Neutron Diffraction Data

Using an iterative approach with the MAUD software package, a consistent and stable operating route was developed to process neutron diffraction data. Specific values including lattice parameters derived from x-ray diffraction (XRD) and the Debye-Waller thermal attenuation factor were required to do so, and were found with additional investigations. All experimental datasets obtained from LANSCE-HIPPO were run through the updated processing route, and results exported into the MATLAB MTEX plugin for quantification. An important detail to note is that both α-Ti and β-Ti texture information was generated, but only α-Ti information is reported here. This is due to a relatively low phase fraction of β-Ti from each specimen (below the required 5 vol % value for sufficient neutron diffraction signal) reducing the confidence in any calculated results.

The MATLAB-MTEX plugin generates recalculated pole figures (**Figure 36.3)** and orientation distribution functions (ODF's) (**Figure 36.4**) giving semi-quantitative and quantitative texture information respectively. Preferred orientations for each diffraction experiment, from here on referred to as texture components, were extracted from ODF's and relative volume fractions of each texture component evaluated. Such a calculation allows for a quantitative comparison between each experiment by observing changes in component volume fraction as a function of scan strategy and build height. This avoids semi-quantitative interpretations of texture information as associated with pole figures and can also illustrate any fiber textures present within the material.

Initial processing indicated a suspected basal fiber texture present in all three specimens as seen in **Figure 36.5**, but further work on the matter has been temporarily halted. This is due to issues in assumed symmetries for pole figure and ODF generation and how these must be reconciled with literature assumptions as described below.

36a.3.2 Crystallographic Texture Review for Titanium Alloys

In order to provide context for the results collected from ODF's, a second literature review was completed for Ti-6Al-4V and similar systems. The primary objective of this search was to identify previously reported texture components in both AM and traditional processing studies, and compare these values to those found in this work. In many material systems, specific texture components indicate distinct microstructural evolution phenomena and give insight into material changes during processing (e.g., recrystallization). Such insight would assist in controlling the microstructure of metallic AM builds, and bring AM one step closer to creating born-ready components.

Comparisons of texture components found in literature to those calculated in MTEX demonstrated noticeable differences with minimal to no overlap for all experiments. Further investigation determined most studies (both AM and traditional manufacturing) imply what is known as an orthotropic specimen symmetry on their texture analysis, assuming a statistical symmetry due to processing of the material (e.g., rolling). Such an assumption is supported by

the presence of an apparent symmetry in pole figures and texture components which repeat at constant intervals throughout an ODF.

Such symmetry and periodicity is not clearly seen in this **Figure 36.4** or **Figure 36.5** however, and suggests a triclinic specimen symmetry may be more applicable for all three specimens. This also presents the possibility the directional build process of AM may not be truly "orthorhombic" due to the lack of symmetry present *within* each build layer, indicating a change in analysis standards is required. Further work is needed to establish the validity of this statement and also confirm whether or not a triclinic specimen symmetry is indeed accurate for the specimens being tested here.

36a.4 Plans for Next Reporting Period

Future work will focus on finishing the texture component analysis of neutron diffraction data, publishing a summary of this work, and developing/publishing a standard operating procedure for processing neutron diffraction data.

- Determine if orthorhombic or triclinic specimen symmetry is appropriate for one, multiple, or all neutron diffraction experiments completed.
- Publish texture component paper in Q3 or Q4-2019.
- Develop instructional and explanatory documentation (video tutorials and documents) for using MAUD software package. A current standard operating procedure has yet to be defined, leading to large degrees of volatility and low confidence in some crystallographic texture studies seen in literature.

36a.5 References

[36.1] Dutta, B., Froes, F.H. (Sam), 2017. The Additive Manufacturing (AM) of titanium alloys. Metal Powder Report 72, 96–106. https://doi.org/10.1016/j.mprp.2016.12.062

[36.2] Frazier, W.E., 2014. Metal Additive Manufacturing: A Review. Journal of Materials Engineering and Performance 23, 1917–1928. https://doi.org/10.1007/s11665-014-0958-z

[36.3] Liu, S., Shin, Y.C., 2019. Additive manufacturing of Ti6Al4V alloy: A review. Materials & Design 164, 107552. https://doi.org/10.1016/j.matdes.2018.107552

[36.4] Sames, W.J., List, F.A., Pannala, S., Dehoff, R.R., Babu, S.S., 2016. The metallurgy and processing science of metal additive manufacturing. International Materials Reviews 61, 315–360. https://doi.org/10.1080/09506608.2015.1116649

[36.5] Al-Bermani, S.S., Blackmore, M.L., Zhang, W., Todd, I., 2010. The Origin of Microstructural Diversity, Texture, and Mechanical Properties in Electron Beam Melted Ti-6Al-4V. Metallurgical and Materials Transactions A 41, 3422–3434. https://doi.org/10.1007/s11661-010-0397-x

[36.6] Brice, C.A., Tayon, W.A., Pilchak, A.L., 2014. Texture Development in Titanium Components Made by Additive Manufacturing. San Diego 16.

[36.7] Butler, T.M., Brice, C.A., Tayon, W.A., Semiatin, S.L., Pilchak, A.L., 2017. Evolution of Texture from a Single Crystal Ti-6Al-4V Substrate During Electron Beam Directed Energy Deposition. Metallurgical and Materials Transactions A 48, 4441–4446. https://doi.org/10.1007/s11661-017-4219-2

[36.8] Chandramohan, P., 2019. Laser additive manufactured Ti-6Al-4V alloy: Texture analysis. Materials Chemistry and Physics 226, 272–278. https://doi.org/10.1016/j.matchemphys.2019.01.035

[36.9] Körner, C., 2016. Additive manufacturing of metallic components by selective electron beam melting — a review. International Materials Reviews 61, 361–377. https://doi.org/10.1080/09506608.2016.1176289

[36.10] Murr, L.E., 2015. Metallurgy of additive manufacturing: Examples from electron beam melting. Additive Manufacturing 5, 40–53. https://doi.org/10.1016/j.addma.2014.12.002

[36.11] Tan, X., Kok, Y., Toh, W.Q., Tan, Y.J., Descoins, M., Mangelinck, D., Tor, S.B., Leong, K.F., Chua, C.K., 2016. Revealing martensitic transformation and α/β interface evolution in electron beam melting three-dimensional-printed Ti-6Al-4V. Scientific Reports 6. https://doi.org/10.1038/srep26039

[36.12] Chastand, V., Tezenas, A., Cadoret, Y., Quaegebeur, P., Maia, W., Charkaluk, E., 2016. Fatigue characterization of Titanium Ti-6Al-4V samples produced by Additive Manufacturing. Procedia Structural Integrity 2, 3168–3176. https://doi.org/10.1016/j.prostr.2016.06.395

[36.13] Juechter, V., Scharowsky, T., Singer, R.F., Körner, C., 2014. Processing window and evaporation phenomena for Ti–6Al–4V produced by selective electron beam melting. Acta Materialia 76, 252–258. https://doi.org/10.1016/j.actamat.2014.05.037

[36.14] Kobryn, P.A., Semiatin, S.L., 2001. The laser additive manufacture of Ti-6Al-4V. JOM 53, 40–42. https://doi.org/10.1007/s11837-001-0068-x

[36.15] Nandwana, P., Lee, Y., Ranger, C., Rollett, A.D., Dehoff, R.R., Babu, S.S., 2019. Post-processing to Modify the α Phase Micro-Texture and β Phase Grain Morphology in Ti-6Al-4V Fabricated by Powder Bed Electron Beam Melting. Metallurgical and Materials Transactions A 50, 3429–3439. https://doi.org/10.1007/s11661-019-05247-4

[36.16] Thijs, L., Verhaeghe, F., Craeghs, T., Humbeeck, J.V., Kruth, J.-P., 2010. A study of the microstructural evolution during selective laser melting of Ti–6Al–4V. Acta Materialia 58, 3303–3312. https://doi.org/10.1016/j.actamat.2010.02.004

[36.17] Xu, W., Brandt, M., Sun, S., Elambasseril, J., Liu, Q., Latham, K., Xia, K., Qian, M., 2015. Additive manufacturing of strong and ductile Ti–6Al–4V by selective laser melting via in situ martensite decomposition. Acta Materialia 85, 74–84. https://doi.org/10.1016/j.actamat.2014.11.028

[36.18] Yang, J., Yu, H., Yin, J., Gao, M., Wang, Z., Zeng, X., 2016. Formation and control of martensite in Ti-6Al-4V alloy produced by selective laser melting. Materials & Design 108, 308–318. https://doi.org/10.1016/j.matdes.2016.06.117

[36.19] Pesach, A., Tiferet, E., Vogel, S.C., Chonin, M., Diskin, A., Zilberman, L., Rivin, O., Yeheskel, O., Caspi, E.N., 2018. Texture analysis of additively manufactured Ti-6Al-4V using neutron diffraction. Additive Manufacturing 23, 394–401. https://doi.org/10.1016/j.addma.2018.08.010

[36.20] Vogel, S.C., Takajo, S., Kumar, M.A., Caspi, E.N., Pesach, A., Tiferet, E., Yeheskel, O., 2018. Ambient and High-Temperature Bulk Characterization of Additively Manufactured Ti-6Al-4V Using Neutron Diffraction. JOM 70, 1714–1722. https://doi.org/10.1007/s11837-018-3038-2

36a.6 Figures and Tables

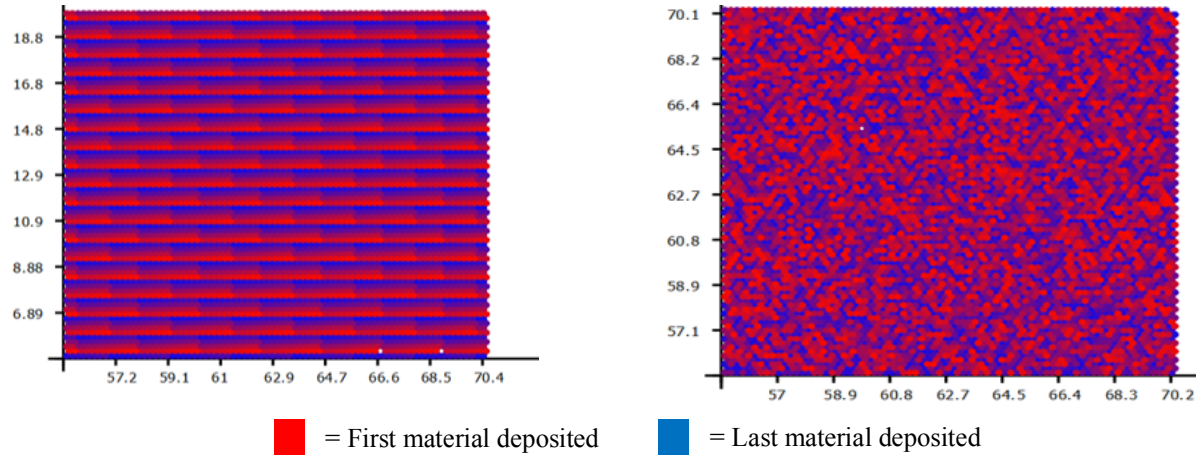

Figure 36.1: Illustrations of the two spot deposition scan strategies Dehoff (left) and Random (right) implemented here.

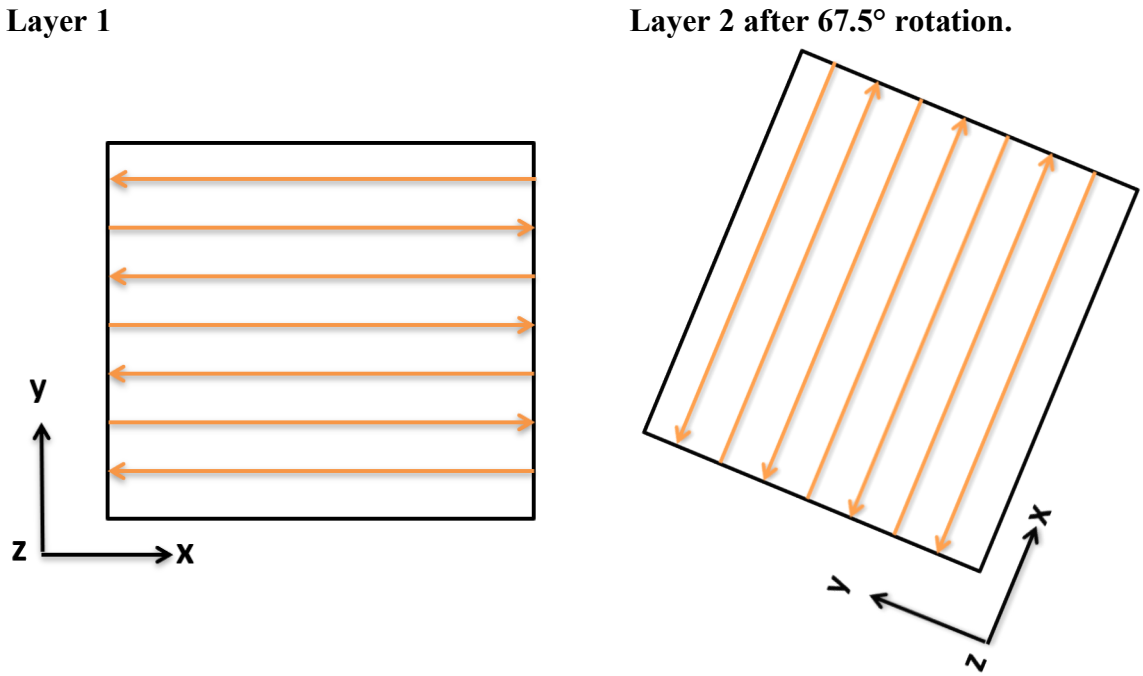

Figure 36.2: Illustration of the Raster scan strategy implemented here. Note the 67.5° rotation between layers incorporated into this build process (right).

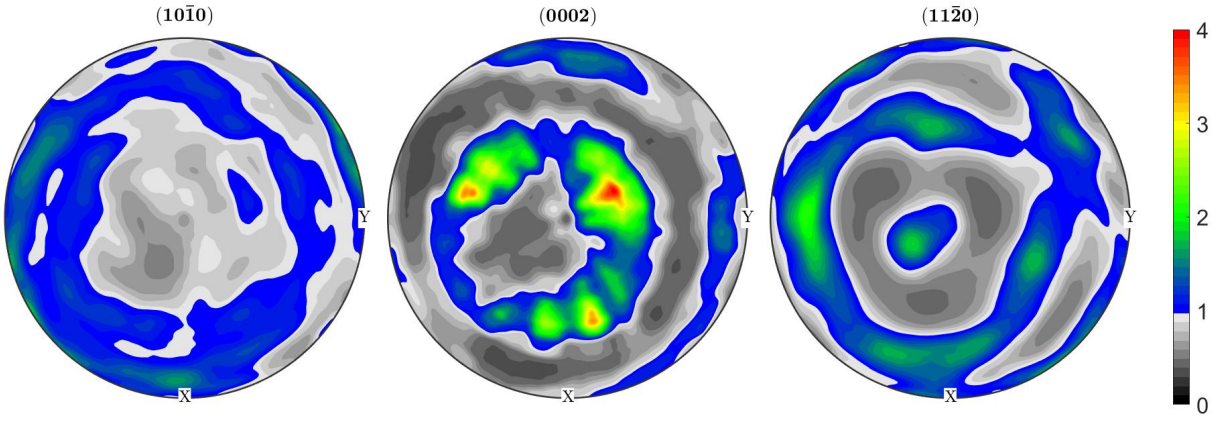

Figure 36.3: Recalculated pole figures for a neutron diffraction experiment of the Random scan strategy specimen. Taken 2 mm from the top of the build geometry.

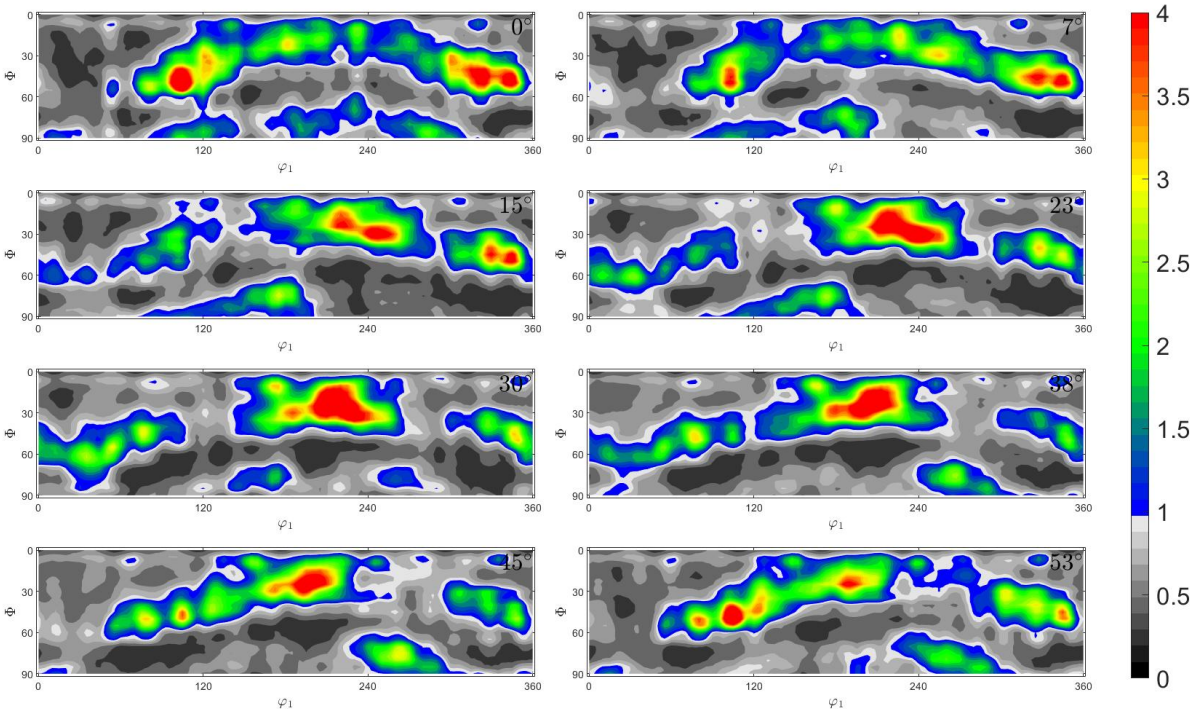

Figure 36.4: Orientation distribution function of the same experiment present in **Figure 36.3**. Note the primary texture components (regions of red coloration) present throughout a suspected HCP basal fiber texture.

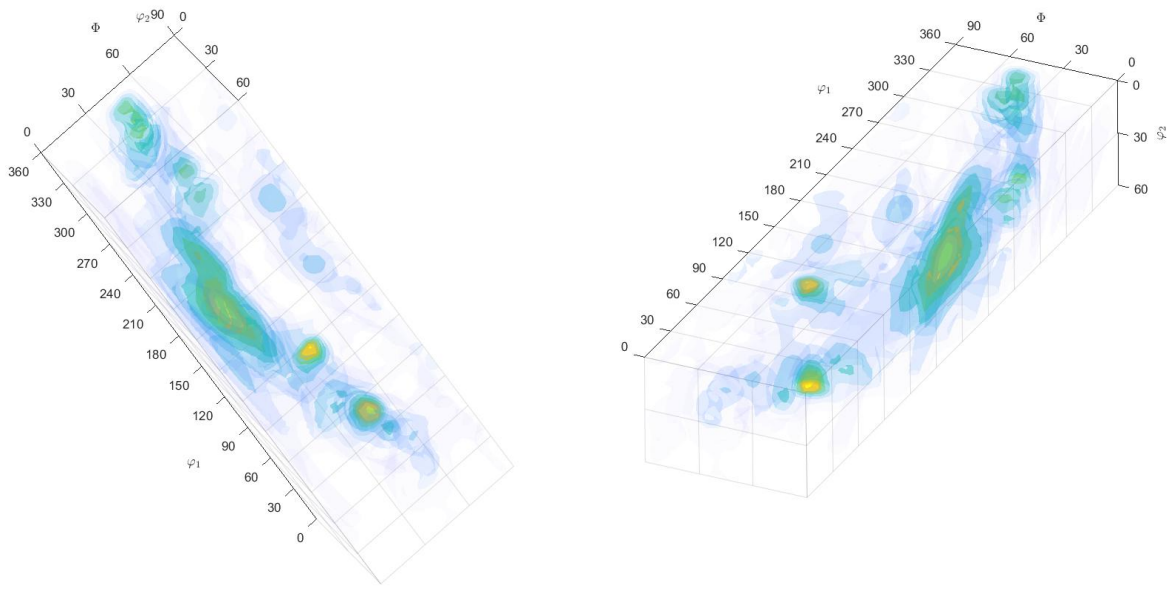

Figure 36.5: 3D ODF illustrating the fiber texture observed in two-dimensional slices in **Figure 36.4** from assorted angles. Views are selected to help develop perspective on the fiber texture's behavior in 3D.